buildings

MDPI

Article

Study on Crystallization Mechanism of Asphalt Mixture in Bridge Deck Pavement

Chuanxi Luo [1,2,*], Duanyi Wang [1], Jian Li [2] and Jun He [1,2]

[1] School of Civil Engineering and Transportation, South China University of Technology, Guangzhou 510000, China; jtcdywang@scut.edu.cn (D.W.); 18825181976@163.com (J.H.)
[2] Xiaoning Institute of Roadway Engineering, Guangzhou 510000, China; m15738523861@163.com
* Correspondence: ctlcx@mail.scut.edu.cn; Tel.: +86-18825181976

Abstract: This study focuses on unknown crystal precipitates from an asphalt mixture used in bridge deck pavement layers. X-ray fluorescence spectroscopy was used to analyze the composition and source of crystals in the asphalt mixture used in bridge deck pavement, and infiltration tests, porosity tests, splitting tests and multi-wheel rutting tests were carried out to determine the precipitation area and non-precipitation area to explain the influence of crystals on the road performance of an asphalt pavement. A nuclear-free densitometer and 3D ground-penetrating radar (3D GPR) were used to detect the porosity and thickness uniformity of the whole section to study the formation mechanism of crystals. The results showed that the main components of crystals were water molecules, while the rest mainly came from machine-made sand, and there was no significant difference in pavement performance in the areas where crystals precipitated. The crystals were mainly caused by rainwater penetrating into the pavement through coarse segregation areas and collecting in the depression of the lower bearing layer. Under high temperature, the solution precipitated out of the pavement and formed crystals.

Keywords: asphalt mixture; pavement; crystals; composition analysis

check for updates

Citation: Luo, C.; Wang, D.; Li, J.; He, J. Study on Crystallization Mechanism of Asphalt Mixture in Bridge Deck Pavement. *Buildings* **2023**, *13*, 1527. https://doi.org/10.3390/buildings13061527

Academic Editors: Andrea Baliello and Di Wang

Received: 25 April 2023
Revised: 30 May 2023
Accepted: 8 June 2023
Published: 14 June 2023

Copyright: © 2023 by the authors. Licensee MDPI, Basel, Switzerland. This article is an open access article distributed under the terms and conditions of the Creative Commons Attribution (CC BY) license (https://creativecommons.org/licenses/by/4.0/).

1. Introduction

After the construction of the structure layer of the asphalt mixture used in a bridge deck pavement is completed, it experiences high temperatures and exposure to rainy weather, causing white or light yellow crystals to precipitate on its surface, as shown in Figure 1. The crystals are distributed in blocks, and their contour is similar to that of liquid flow, with an area of about 0.01–0.2 m^2. The crystals have a certain thickness and can be easily scraped off. The source and influence of these crystals on the performance of existing pavements have been puzzling road workers and have, at one point, caused the project to stop. This paper focuses on the source of these crystals, their influence on the properties of mixtures and their formation mechanism.



(**a**) (**b**) (**c**)

Figure 1. Morphology of crystals. (**a**) Crystal profile; (**b**) crystal side detail; (**c**) crystal front detail.

In the past, the asphalt mixture used in the bridge deck pavement often had crystals appearing after alkaline flooding, which were white or yellow water-insoluble attachments distributed in flakes or scattered spots [1–3]. The crystals have a certain thickness, are powder-like crystals, and most of them are soluble in water. There are the obvious differences in morphology and solubility between the two substances. The main reason for flooding is the coarse segregation of the asphalt mixture, which leads to rainwater infiltrating into the materials dissolved in the bridge deck pavement and precipitating through connected gaps. The flooding of the bridge deck pavement indicates that there are connected gaps in the pavement structure layer, and early pit diseases are prone to occur during pavement maintenance [4–7]. Relevant research shows that when rainwater accumulates between pavement and the cement concrete of a bridge deck, it may cause a hydrodynamic scouring phenomenon when a traffic load is present, which would lead to a failure in the connection between the pavement and bridge deck, and even delamination [8–10]. According to the research results of relevant researchers, a relatively dense asphalt mixture has been applied in the bridge deck pavement [11–14]. In recent years, alkaline flooding of the bridge deck pavement has not occurred as often [15–18]; however, the crystal phenomenon has occurred in the asphalt pavement of newly built subgrade sections after alkaline flooding, though there is no relevant report on the diseases caused by alkaline flooding in subgrade sections [19–21]. With the increasing frequency of alkaline flooding, the diseases caused by flooding are being paid attention to by road workers [22]. Some researchers think that the flooding of the structural layer is only the precipitation of substances in the pavement layer, which has little correlation with the performance of the structural layer, and that the early damage was mainly caused by the connecting gaps [23,24]; therefore, some scholars believe that the phenomenon of alkaline flooding can be solved only by replacing the structural layer with a denser asphalt mixture [25–27]. The fact of the matter is, however, that the phenomenon of alkaline flooding has decreased, but it still exists [28–31]. There is still no complete research result on the formation mechanism of alkaline flooding.

Huang Zhiyong et al. showed that alkaline flooding is different from asphalt, aggregate and dust flooding, cannot be washed away by high-pressure water and has a certain adhesion strength [32,33]. Li Weixiong et al. carried out chemical analyses of alkaline flooding substances and found that the main substances were $CaCO_3$, $Mg(OH)_2$ and $CaCO_3$ [34–36]. Related scholars have carried out a series of studies on the phenomenon of alkaline flooding, but crystallization has not been the focus in pavement engineering [37,38]. There were some detailed research results on the precipitation of crystals in soil. Larsen studied the mechanism of calcium carbonate scaling through laboratory core flow tests based on the theory of crystal growth dynamics [39]. Charpentier studied the crystallization of calcium carbonate and sulfuric acid in subsea downhole equipment through dynamic tests [40]. Sadra studied the kinetics of calcium sulfate crystals through experiments [41]. The regularity of groundwater crystallization and its influence on the stability of a high slope were analyzed by Gao Chunqun [42]. Liu Yuyang carried out research on the occurrence rule and crystallization path of crystals in tunnel drainage systems surrounded by calcium-rich rock [43]. Wu Yuzhe analyzed the component characteristics and sources of the porous crystallites in a loess tunnel and proposed that the crystallites were mainly Ca and Mg ions [44]. Cement concrete, similarly to asphalt concrete, also experienced a crystallization phenomenon. When the phenomenon of bad crystallization was too strong, it directly affected the performance of concrete [45,46]. Asphalt concrete may have the same problem. At the present stage, the chemical composition, mechanism and influence on the performance of the pavement layer of the asphalt-mixture bridge deck are not clear.

X-ray fluorescence spectroscopy was used to analyze and compare the composition differences between raw materials, machine-made sand, bridge deck milling waste and crystals, and to study the composition and source of crystals. An infiltration test, porosity test, splitting test and multi-wheel rutting test were carried out for determining the crystalline area and non-crystalline area, and the differences between them were analyzed

to introduce the pavement performance of the crystalline area. Finally, the porosity and thickness uniformity were analyzed using a nuclear-free densitometer and 3D GPR, and the formation mechanism of crystals was studied.

2. Methods

2.1. Composition and Source Analysis of Crystals

Crystals appeared 2–3 days after the completion of the bridge deck pavement construction, during which large-scale rainfall and high temperature weather occurred. After the bridge deck pavement construction was completed, traffic was closed off without interference from external factors. The possibility of foreign substances was eliminated by analyzing the distribution law and adhesion of crystals on site. Combined with the external contour of the bridge deck pavement surface, crystals were formed by liquid crystals and the composition of crystals from the bridge deck pavement structure. The structure consists of an asphalt surface layer, waterproof adhesive layer, adhesive layer and milled bridge deck integral layer, as shown in Table 1. Relevant research shows that the phenomenon of alkaline flooding mainly comes from gravel dust in the waterproof bonding layer and milling dust on the bridge deck. The gravel of the waterproof bonding layer of this project must be dusted by a mixing plant and wrapped with 0.3% asphalt, which can eliminate the possibility of crystallization caused by gravel dust. In order to analyze the composition and source of crystals, X-ray fluorescence spectrometry was used to compare and analyze the composition of raw materials, machine-made sand, bridge deck milling waste and crystals.

Table 1. Bridge deck pavement structure.

Layer	Type
Upper pavement	SMA-13 (SBS modified asphalt)
Lower pavement	GAC-20 (SBS modified asphalt)
Waterproof adhesive layer	Synchronous macadam seal (SBS modified asphalt)
Adhesive layer	Modified emulsified asphalt

2.2. Influence Analysis of Pavement Performance

In order to study the influence of crystal on the performance of the pavement, an infiltration test, core sample porosity test, splitting test and multi-wheel rutting test were carried out for the crystal and non-crystal area, respectively, and the performance difference between the crystal and non-crystal area was obtained. Among them, an infiltration test and core sample porosity test were used to analyze the difference in pavement compactness and study the compactness of the crystal precipitation area [33,34]. The core sample splitting test was used to explain the difference of mechanical properties, and study the influence of crystal precipitation on mechanical properties. A multi-wheel rutting test of core samples was used to introduce the difference in high temperature stability, and study the influence of crystal precipitation on rutting deformation resistance. See Figure 2 for the schematic diagram.

2.3. Analysis of Precipitation Mechanism of Crystals

The uniformity analysis of the whole section was carried out using a non-nuclear density meter and 3D GPR, where the non-nuclear density meter detected the porosity distribution, and studied the corresponding relationship between the porosity segregation area distribution position and the crystal precipitation area distribution position. Three-dimensional GPR uses the principle of electromagnetic wave propagation to detect the thickness distribution of the full section of a pavement, and the calculation model is shown in Equation (1). The corresponding relationship between the distribution position of the thickness segregation area and the distribution position of the crystal precipitation area was studied, and the mechanism of crystal formation was analyzed.

$$h = \frac{c}{\sqrt{\varepsilon}} \frac{t}{2} \tag{1}$$

where c is the speed of light, and the theoretical value is 3×10^8 m/s; ε is the dielectric constant of the structural layer, calculated by Equation (2); t is the two-way propagation time of the electromagnetic wave in the structural layer.

$$\varepsilon = \frac{c^2 t_H{}^2}{4H^2} \tag{2}$$

where H is the height of the core sample and t is the two-way propagation time of the electromagnetic wave in the core sample.

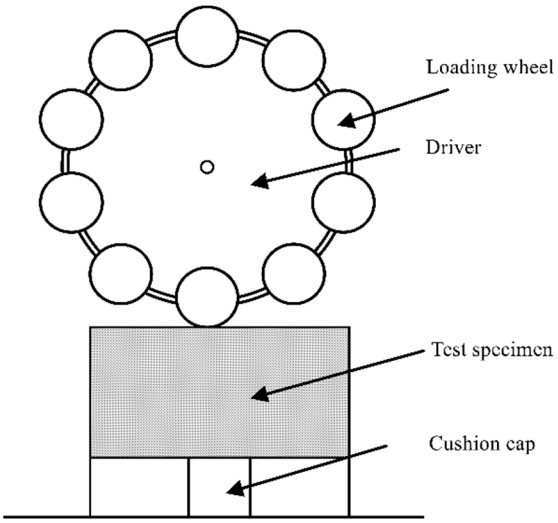


Figure 2. Schematic diagram of multi-wheel rutting test.

3. Experimental Plan

3.1. Raw Materials

The asphalt used in the waterproof bonding layer of the bridge deck pavement and the lower pavement is SBS-modified asphalt, and the test index is shown in Table 2. Limestone was used as aggregate in the lower pavement, and the test index of fine aggregate is shown in Table 3. The lower pavement adopts a skeleton-dense asphalt mixture, and the gradation is shown in Figure 3. The test methods refer to "Test Regulations for Asphalt and Asphalt Mixture of Highway Engineering" (JTG E20-2011).

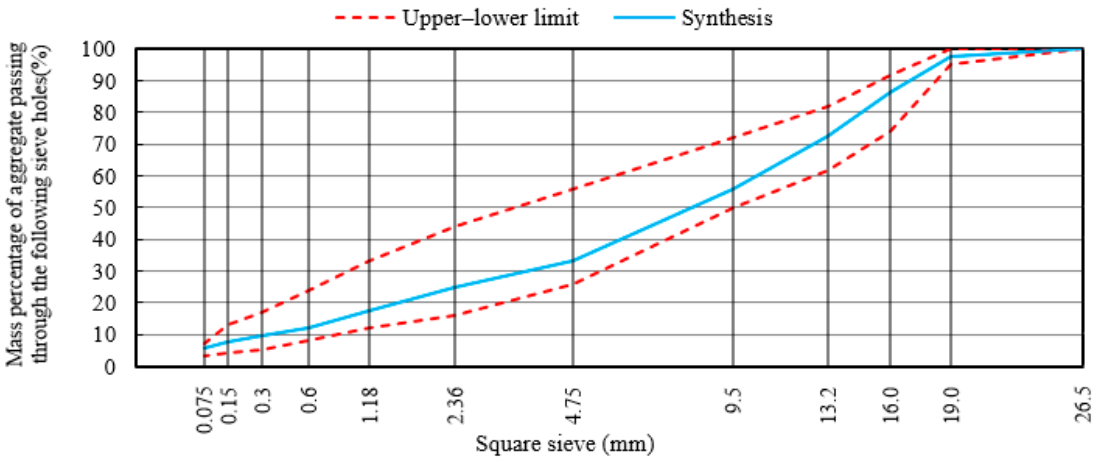


Figure 3. Mineral aggregate gradation of lower pavement's asphalt mixture.

Table 2. Index of SBS-modified asphalt.

Pilot		Test Results
Penetration 25 °C, 100 g, 5 s, (0.1 mm)		49
Ductility 5 °C, 5 cm/min, (cm)		33
Softening point, $T_{R\&B}$ (°C)		88
Solubility (%)		99.8
Storage stability: 163 °C; 48 h; softening point difference, °C		0.8
Elastic recovery 25 °C, %		96
Kinematic viscosity at 135 °C (Pa·s)		2.42
Rolling thin film oven test (RTFOT) Residue (163 °C, 85 min)	Quality change (%)	0.016
	Ductility 5 °C, 5 cm/min, (cm)	22
	Penetration ratio (%)	77.7

Table 3. Fine aggregate index.

Test Index	Unit	Test Results
Apparent relative density	—	2.947
Rigidity (>0.3 mm part)	%	2.7
Sand equivalent	%	69
Methylene blue value	g/kg	0.9
Angularity (flow time)	s	38.7

3.2. Test Plan of X-ray Fluorescence Spectrometry

The sample preparation carried out via X-ray fluorescence spectrometry usually adopts a tableting method or melting method. The tablet pressing method is relatively simple, but its particle size effect is obvious, and the accuracy and repeatability of test results are poor. The melting method can greatly reduce the particle size effect, but it needs a high temperature for melting, so it is impossible to detect H_2O, C and other related elements. According to the characteristics of the samples, the melting method was selected for composition analysis. The machine-made sand, bridge deck milling materials and crystals were analyzed via X-ray fluorescence spectrometry.

First, amounts of 6.0 g of a mixed flux and 0.6 g of crystallites were placed in a platinum crucible and carefully mixed with a glass rod. Then, 1 mL of a lithium nitrate solution was uniformly added, placed on the sample rack of the high-frequency fusion machine, oxidized at 500 °C for 5 min, then fused at 1000 °C for 2 min, and then fused by swinging for 8 min. During the melting process, a small amount of ammonium iodide was added every 2–3 min. It was added for the last time 2 min before the end. After melting, the molten material was poured into a preheated mold carefully. After cooling, the glass sheet was removed and marked. The glass plate containing the crystal was placed in the X-ray fluorescence spectrometer to obtain the chemical elements of the crystal and their proportions.

3.3. Test Plan of Pavement Performance

The morphology of crystals was observed. Combined with the parameters of transverse and longitudinal slopes, the precipitation points of crystals were determined. This point was taken as the center, and a water seepage test was carried out and so was coring; see Figure 4 for the test position. Among them, the four test points were arranged in combination with the combined slope of transverse and longitudinal slopes, so that the test points were at the highest point and the lowest point in the direction of the combined slope to analyze the relationship between the precipitation point and the combined slope.

The other two test points were 90° away from the highest and low points, respectively, and the four test points were 0.3 m away from the central test point. According to the 6 crystal precipitation areas, the water permeability coefficient was detected according to the Code for On-site Test of Highway Subgrades and Pavements (JTG 3450-2019), and the porosity was measured by coring.

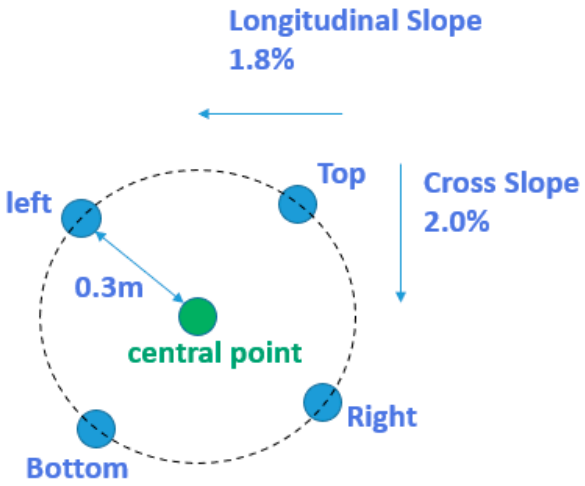


Figure 4. Schematic diagram of test position.

According to the core samples in the above-mentioned three crystal areas, the splitting strength test was carried out according to the Test Code for Asphalt and Asphalt Mixture in Highway Engineering (JTG E20-2011), and the test temperature was 25 °C. Based on the core samples in the other three crystal areas, multi-wheel rutting tests were carried out at 60 °C, and the rutting depth was measured by running the small wheels 16,000 times.

3.4. Nuclear-Free Density and 3D GPR Test Plan

A PQI380 nuclear-free densimeter was used to carry out the determination of the porosity distribution of the asphalt structural layer in the whole section. Starting from 0.5 m away from the edge of the bridge deck pavement, the horizontal interval was 0.5 m, the vertical interval was 0.5 m, and the test points were set with a test length of 20 m and a total of 1120 test points. See Figure 5 for the schematic diagram of the test. Three-dimensional GPR was used to detect the thickness of the crystallization area. The longitudinal and transverse interval of the data output was 0.15 m, and 13,266 points of thickness data were the output.

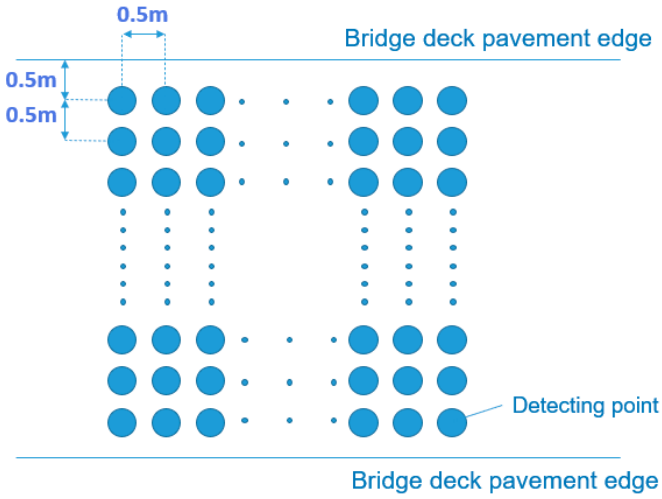


Figure 5. Schematic diagram of test of nuclear-free densimeter.

4. Results and Analysis

4.1. Source Analysis of Crystals

See Figure 6 for the test results of the machine-made sand, bridge deck milling waste and crystals obtained via X-ray fluorescence spectrometry.

As can be seen from Figure 6a, CaO accounts for 54.95% of the composition of the machine-made sand, while the LOI accounts for 42.91%, where the LOI is the ignition loss caused by melting and sample preparation before conducting the X-ray fluorescence spectrometry analysis. The machine-made sand of the asphalt mixture is limestone, and its main component is $CaCO_3$. According to the chemical characteristics of $CaCO_3$, it produces a decomposition reaction at high temperatures, as shown in Equation (3).

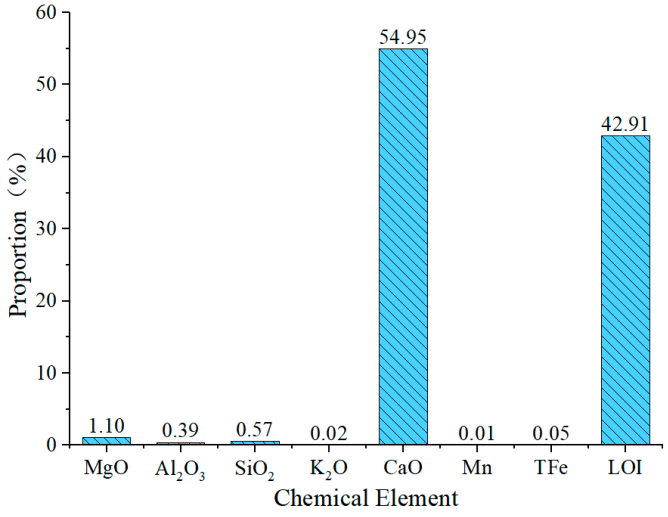
$$CaCO_3 \xrightarrow{\text{High Temperature}} CaO + CO_2 \quad (3)$$

$CaCO_3$ decomposed at high temperatures to form CaO and CO_2, in which CO_2 is gaseous and volatilizes during melting and sample preparation, thus producing ignition failure stress. According to the law of conservation of mass, after $CaCO_3$ was decomposed into CaO and CO_2, the mass ratio of CaO to CO_2 was 56:44, while the ratio of CaO to LOI in machine-made sand was 56:44, indicating that CO_2 is the main component in the LOI. As can be seen from Figure 6b, SiO_2 accounts for 46.16%, CaO accounts for 26.58% and the LOI accounts for 17.28% in bridge deck milling waste. As can be seen from Figure 6c, the LOI accounts for 98.95%, Al_2O_3 accounts for 0.23%, SiO_2 accounts for 0.43%, and CaO accounts for 0.23%. A total of 98.95% of crystals evaporated in the gaseous state during sample preparation, and the proportion of combined CaO was only 0.23%, so the volatile gas could not be CO_2-decomposed by $CaCO_3$ at high temperatures. Combined with the composition of the asphalt mixture, considering that H_2O and C cannot be detected via X-ray fluorescence spectrometry under melting and sample preparation, the crystals are dissolved in pure water. Observation shows that most crystals are soluble in water, with only a small amount of precipitates. Combined with the characteristic that the C molecule of organic matter (asphalt) does not melt in pure water, it can be judged that the main component of the LOI is H_2O.

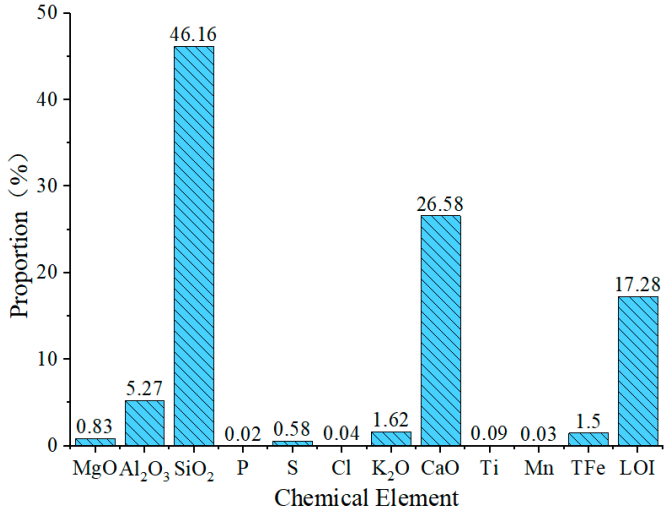
Crystal CaO is mainly caused by $CaCO_3$ forming a Ca $(HCO3)_2$ solution under the action of atmospheric CO_2 and rainwater. The chemical reaction is shown in Equation (4), and the solution precipitates out of the surface by connected gaps. With the increase in temperature, $Ca(HCO_3)_2$ decomposes into $CaCO_3$, CO_2 and H_2O, and the chemical equation is shown in Equation (5). $CaCO_3$ exists in the machine-made sand, bridge deck milling waste and crystals, and it is impossible to analyze the source by comparing CaO quality ($CaCO_3$ can decompose to form CaO and CO_2). As can be seen from Figure 6, the composition of bridge deck milling waste includes P, S, Cl and Ti, while the machine-made sand does not contain the above components, and the crystal composition includes S and Cl, but not P and Ti. The milling material is composed of cement concrete, and the water and rainwater of crystals must contain S and Cl elements, so it is impossible to determine the source via the presence of S and Cl elements. P and Ti elements do not appear in crystals in bridge deck milling waste, so it can be preliminarily speculated that crystals mainly come from the machine-made sand. In addition, SiO_2 and Al_2O_3, which have a high content of components in the melted crystals, should exist as silicate and aluminate in the crystals, and both SiO_2 and Al_2O_3 in the machine-made sand and bridge deck milling waste are silicate and aluminate. The ratio of SiO_2 to Al_2O_3 in crystals is 1.87, and that in machine-made sand is 1.46; the ratio of SiO_2 to Al_2O_3 in bridge deck milling waste is 8.76. The element ratio of crystals is relatively close to that of machine-made sand, so it can be assumed that crystals (after deducting water molecules) mainly come from machine-made sand.

$$CaCO_3 + CO_2 + H_2O \rightarrow Ca(HCO_3)_2 \quad (4)$$

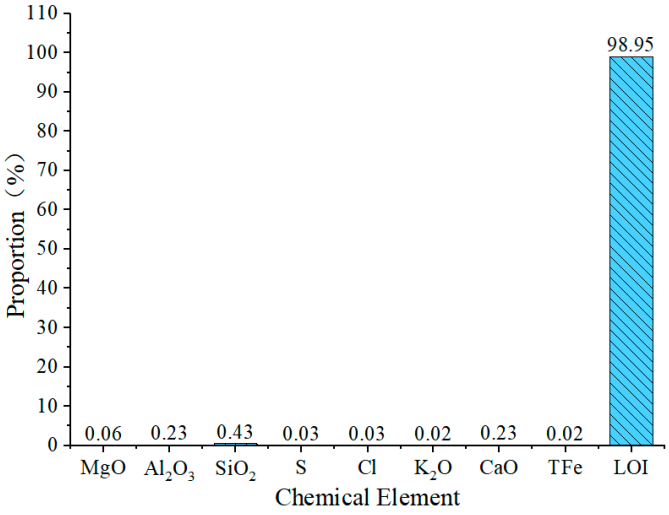
$$Ca(HCO_3)_2 \rightarrow CaCO_3 \downarrow + CO_2 \uparrow + H_2O \quad (5)$$



(**a**)



(**b**)



(**c**)

Figure 6. Test results of fluorescence spectrometry. (**a**) Analysis results of machine-made sand; (**b**) analysis results of bridge deck milling materials; (**c**) analysis results of crystals.

4.2. Road Performance Analysis

See Table 4 for the test results of the road performance indexes of crystals and surrounding areas. The average permeability coefficient of the crystalline precipitation area is 39.5 mL/min, and the average permeability coefficient of the peripheral area is 26.5 mL/min. The permeability coefficient of the crystalline precipitation area is slightly higher than that of peripheral area, but it meets the design requirements. The porosity of the crystalline precipitation area is 4.7%, while the porosity of the peripheral area is 4.2%, and the porosity of crystalline precipitation area is slightly higher than that of the peripheral area. The splitting strength and rutting depth of core samples in the crystallization area are similar to those in the surrounding area, but there is no obvious difference.

Table 4. Performance test results.

Indicators	Position	Average	Difference
Water permeability coefficient (mL/min)	Center point	39.5	−13
	Peripheral average	26.5	
Porosity (%)	Center point	4.7	−0.5
	Peripheral average	4.2	
Splitting strength (MPa)	Center point	0.737	0.034
	Peripheral average	0.771	
Rutting depth (mm)	Center point	1.59	−0.05
	Peripheral average	1.54	

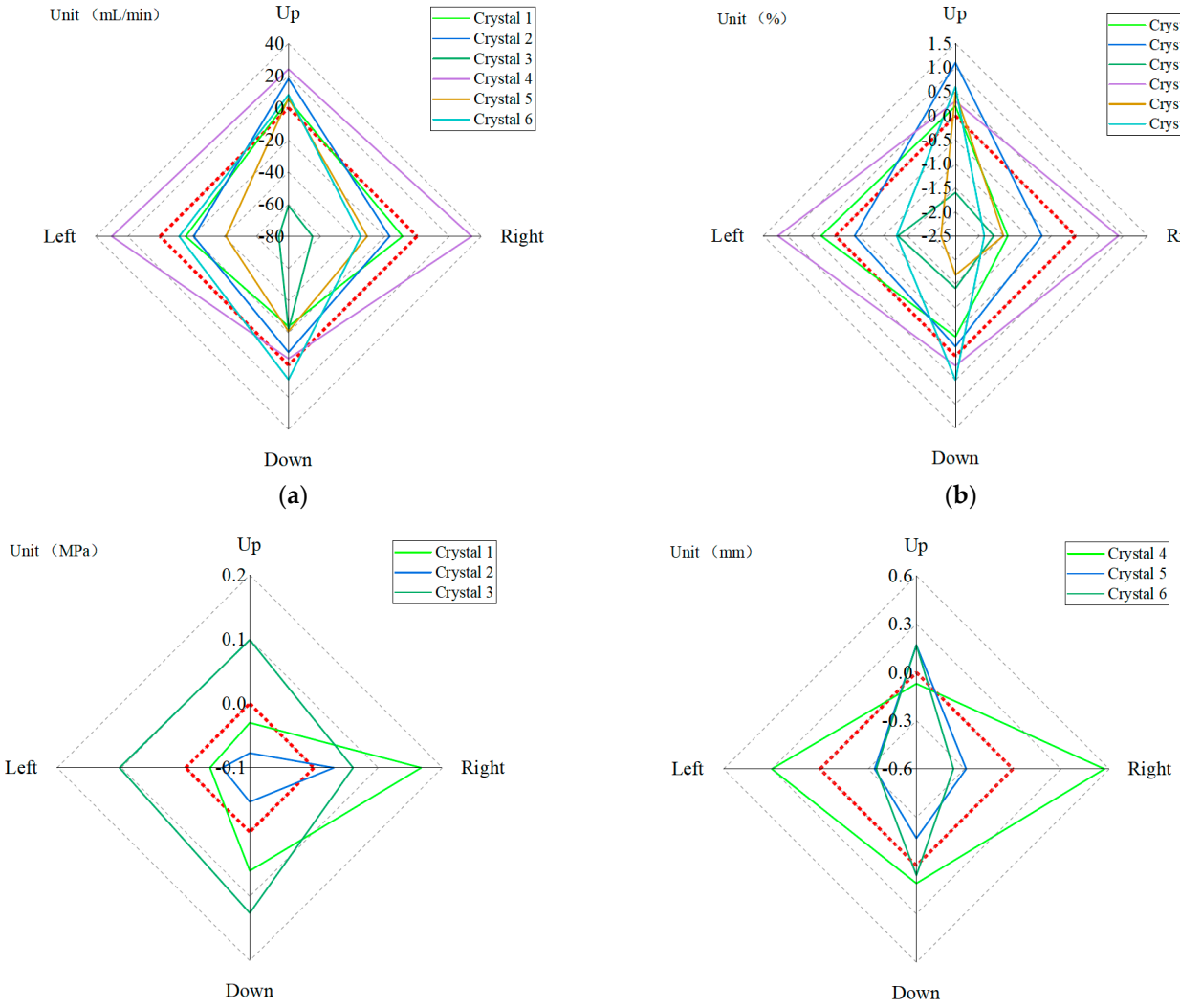
In order to further analyze the performance difference between the crystal precipitation area and the surrounding area, data analysis was carried out for different crystal areas, and the test results of the crystal precipitation area were taken as the reference numbers and compared with the test results of the surrounding area; that is, "test results of the surrounding area-test results of the crystal precipitation area". The calculation results are shown in Figure 7.

From Figure 7a, it can be seen that there are obvious differences between the water permeability coefficient of peripheral areas in different directions and the water permeability coefficient of crystal precipitation areas. The water permeability coefficient of the highest point in the peripheral areas of five crystals is greater than that of the crystal precipitation areas, and the water permeability coefficient of five of the other three directions is smaller than that of crystal precipitation areas. The percolation coefficient of the highest point in the surrounding area is too large, and the percolation coefficient of the surrounding area in other directions is too small, so the percolation coefficient is not the key factor affecting the precipitation of crystals.

As can be seen from Figure 7b, the porosity of the highest point in the surrounding area of five crystals is greater than that in the precipitation area, and the porosity of the lowest point of four crystals is smaller than that in the precipitation area. The void fraction of the highest point is too large and the void fraction of the lowest point is too small in the surrounding area, so the void fraction is not the key factor affecting precipitation.

As can be seen from Figure 7c,d, there is no obvious law in the splitting strength and rutting depth. In order to further study the difference between crystals and surrounding areas, different crystals areas are analyzed separately, as shown in Table 5.

It can be seen from Table 5 that there is no obvious difference in splitting strength and rutting depth between the crystal area and the surrounding area. Fitting analysis was carried out using the core sample's porosity, splitting strength and rutting depth, as shown in Figures 8 and 9.



Note: the gray dotted lines are coordinate grid lines; the red dotted line is the reference line with the coordinate value 0.

Figure 7. Test results of regional properties of different crystals. (**a**) Comparison results of water permeability coefficients; (**b**) comparison results of porosity; (**c**) splitting strength comparison result; (**d**) rutting depth comparison result.

Table 5. Analysis results of splitting strength and rutting depth.

Position	Splitting Strength (MPa)			Rutting Depth (mm)		
	Crystal 1	Crystal 2	Crystal 3	Crystal 4	Crystal 5	Crystal 6
Crystal region	0.723	0.803	0.686	1.32	1.86	1.72
Average value of peripheral area	0.763	0.766	0.783	1.55	1.7	1.6
Difference	6%	−5%	14%	17%	−9%	−7%

It can be seen from Figures 8 and 9 that the splitting strength decreases with the increase in the porosity of the core samples, and the rutting depth increases with the increase in porosity. There is a good relationship model between the splitting strength, rutting depth and porosity, as shown in Equations (6) and (7), which shows that porosity is the main factor affecting splitting strength and rutting depth. Therefore, crystals do not

have a significant impact on the mechanical properties and high temperature stability of the asphalt mixture.

$$y = 1.1 + 0.81x \qquad R^2 = 0.71 \tag{6}$$

$$y = 0.7 + 0.21x \qquad R^2 = 0.65 \tag{7}$$

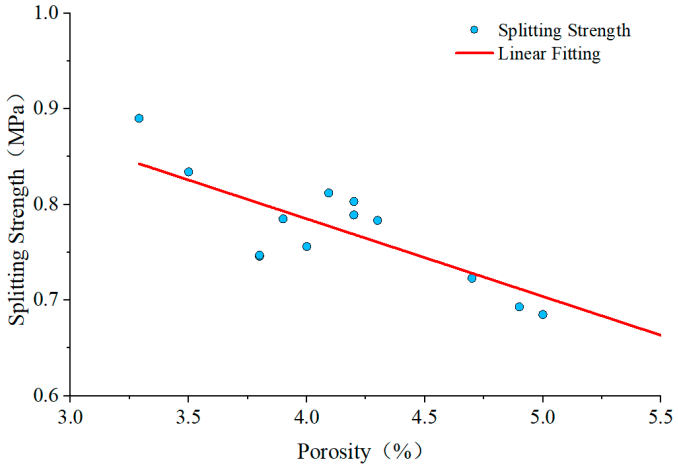


Figure 8. Fitting results of splitting strength and void fraction.

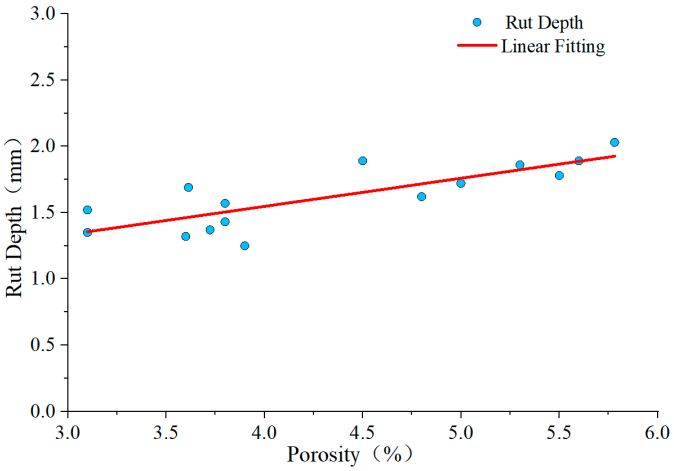


Figure 9. Fitting results of rutting depth and void fraction.

4.3. Nuclear-Free and Radar Test

In order to effectively analyze the spatial distribution of porosity, yellow represents the area with a porosity of less than 3%, green represents that of between 3% and 5%, and red represents an area greater than 5%. See Figure 10 for the porosity test results. It was found that the porosity is too large at the edges of both sides of the road. Because two pavers are used for paving in parallel, there is an obvious segregation phenomenon at the lap joint, which leads to the porosity being too large.

In order to effectively analyze the spatial distribution of thickness, purple is used to represent the area with a thickness greater than 8.8 cm, green represents that between 7.2–8.8 cm, and blue represents a smaller area. See Figure 11 for the thickness test results. It was found that the area with a large thickness is distributed in blocks. Because the interface is a deck pavement, the flatness of the lower bearing layer is not good. When there is a depression in the base surface, the thickness of the pavement will increase abnormally. According to the test results of 3D GPR, there are six basal depression areas in the test range.

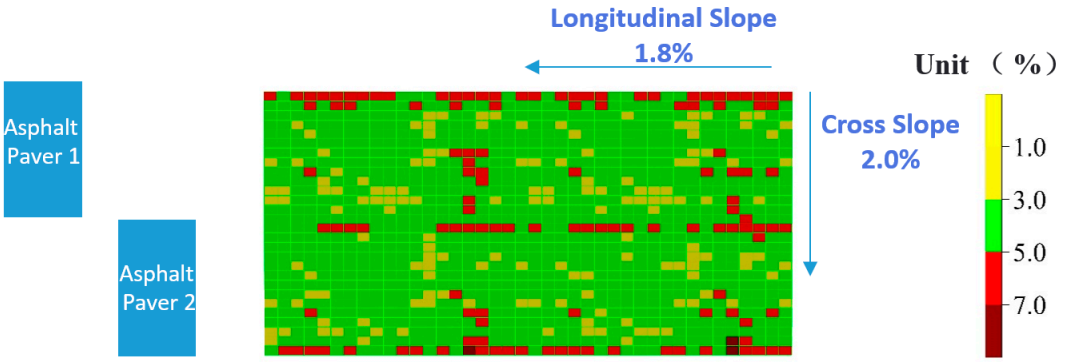


Figure 10. Result of porosity test.

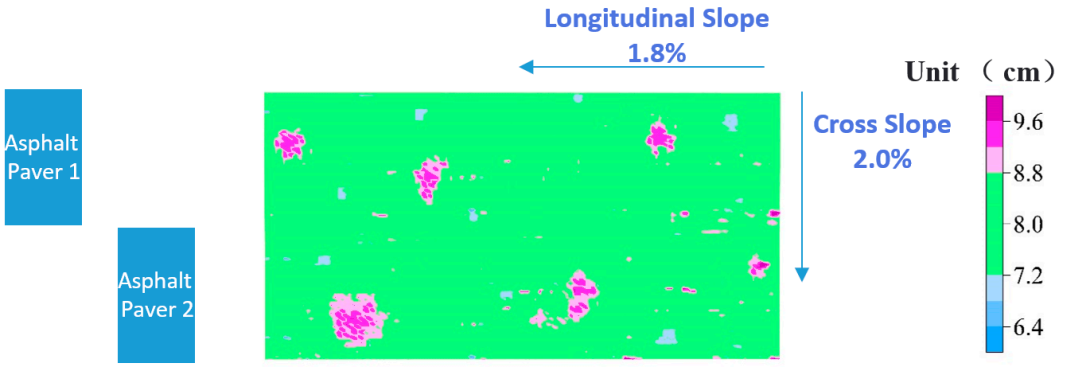


Figure 11. Thickness test results.

In order to further analyze the formation mechanism of crystals, the crystal region, the porosity region and the basal depression region are analyzed. The results are shown in Figure 12. It can be found that crystals precipitate at points A, B, C and F, all of which are located in the basal depression area, and there are areas with large porosity at the high places in the synthesis slope direction. It can be seen that rainwater infiltrates into the pavement structure from the area with large porosity, and then collects to the base depression area through the connecting void, precipitates upward under the action of high temperature, and loses water to form crystals. However, although there are areas with large porosity in the direction of synthetic slope at points D and E, the distance is relatively far, so it is impossible to form connected flow, so it is impossible to collect rainwater.

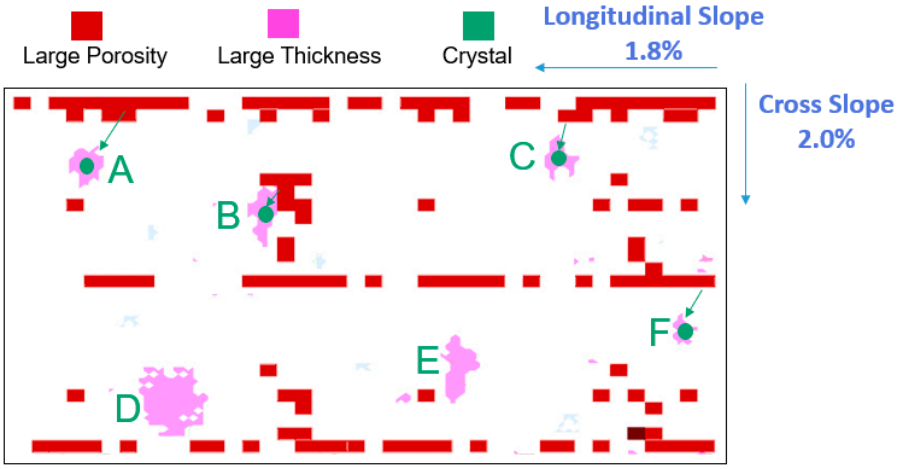


Figure 12. Analysis results of porosity and thickness combination.

In order to avoid crystals in the pavement, the uniformity of pavement construction should be improved as much as possible in the construction process to avoid segregation. For edge segregation and lap segregation areas, rubber wheels can be rolled once more to minimize the connected gap. If a segregation phenomenon is found after construction, emulsified asphalt and other materials can be used to block the connected gap. The flatness of the lower bearing layer of the bridge deck pavement should be improved, and local depressions can be leveled via milling to avoid the accumulation of infiltrated rainwater.

5. Conclusions

In this study, X-ray fluorescence spectroscopy was used to analyze the crystal composition of an asphalt-mixture bridge deck pavement, and the road indexes of the crystal precipitation area and non-precipitation area were detected. Nuclear-free densitometer and 3D GPR were used to detect the porosity and thickness uniformity of the whole section, and the following results were obtained:

(1) In total, 99% of the crystals are composed of H_2O, and the other components with a higher content include Al_2O_3, SiO_2 and CaO.
(2) The crystals (after deducting water molecules) mainly come from machine-made sand.
(3) The water permeability coefficient and porosity in the precipitation area are slightly larger than those in the non-precipitation area, but they all meet the design requirements; for splitting strength and multi-wheel rutting depth, there is no obvious difference between the precipitated area and non-precipitated area.
(4) The formation mechanism of crystals; rainwater penetrates into the pavement through the coarse segregation area, and collects in the depression of the lower bearing layer through the connecting gap. Under the action of high temperature, the solution precipitates out of the pavement surface and undergoes crystallization.
(5) In order to avoid the formation of crystals, the voidage ratio should be properly reduced in the design of the mixture to improve the dense water performance. The construction process should ensure the formation of the bottom bearing layer, to avoid the accumulation of water seepage. At the same time, the uniformity of the pavement should be further improved to ensure the watertight performance of the paving layer.

Through the study in this paper, it was determined that the crystallites come from machine-made sand, but machine-made sand should be wrapped in asphalt in the mixture, and how the infiltration rainwater melts machine-made sand has not been thoroughly analyzed and studied in this paper. In a follow-up study, relevant laboratory experiments can be carried out to reproduce crystallites, and CT technology or standard aggregate can be used to reproduce the whole process of crystallinity formation, so as to further analyze the conditions and requirements of crystallinity.

Author Contributions: Conceptualization, C.L. and D.W.; methodology, C.L.; software, J.L.; validation, C.L., D.W. and J.L.; formal analysis, J.H.; investigation, J.H.; resources, J.H.; data curation, J.L.; writing—original draft preparation, C.L.; writing—review and editing, C.L.; visualization, C.L.; supervision, D.W.; project administration, D.W.; funding acquisition, D.W. All authors have read and agreed to the published version of the manuscript.

Funding: This research was funded by the Natural Science Fund of Guangdong Province, grant number 2019A1515011965, and Natural Science Foundation of China, grant number 51808228.

Data Availability Statement: The data presented in this study are available upon request from the corresponding author.

Acknowledgments: The authors gratefully acknowledge the Natural Science Fund of Guangdong Province, grant number 2019A1515011965, and Natural Science Foundation of China, grant number 51808228.

Conflicts of Interest: The authors declare no conflict of interest.

References

1. Baojun, M. Study on Pavement Quality Control Technology of Asphalt Concrete Bridge Deck of Highway in Mountainous Areas. Master's Thesis, Chang'an University, Xi'an, China, 2020.
2. Hongjun, W.; Yuxia, L.; Jianlin, S. Types and Causes of asphalt pavement damage of cement concrete bridge deck. *Highw. Transp. Sci. Technol. (Appl. Technol. Ed.)* **2014**, *10*, 213–216.
3. Changan, Z. Damage cause analysis and preventive measures of asphalt concrete bridge deck pave-ment. *Gansu Sci. Technol.* **2013**, *29*, 110–111.
4. Yue, F. Study on Color Generation and Decay Mechanism of Asphalt Pavement. Master's Thesis, Fuzhou University, Fuzhou, China, 2019.
5. Cui, P.; Xiao, Y.; Fang, M.; Chen, Z.; Yi, M.; Li, M. Residual Fatigue Properties of Asphalt Pavement after Long-Term Field Service. *Materials* **2018**, *11*, 892. [CrossRef] [PubMed]
6. Karki, P.; Zhou, F. Systematic Method for Quantifying Re-Refined Engine Oil Bottom Content in Binders Using X-Ray Fluorescence Spectroscopy. *Transp. Res. Rec.* **2017**, *2632*, 52–59. [CrossRef]
7. Qian, G.P.; Li, S.J.; Yu, H.N.; Gong, X.B. Interlaminar Bonding Properties on Cement Concrete Deck and Phosphorous Slag Asphalt Pavement. *Materials* **2019**, *12*, 1427. [CrossRef]
8. Muyu, L.; Luy, W.; Chunling, Y.; Juan, T. An experimental study on fading and whitening of asphalt pavement in Guangxi Region. *Smart Cities* **2021**, *7*, 31–32. [CrossRef]
9. Lei, Y.; Hu, X.D.; Wang, H.N.; You, Z.P.; Zhou, Y.L.; Yang, X. Effects of vehicle speeds on the hydrodynamic pressure of pavement surface: Measurement with a designed device. *Measurement* **2017**, *98*, 1–9. [CrossRef]
10. Liang, B.; Jiang, B.L. Study on Composition and Simulation Analysis of Traffic Loads in Submerged Floating Tunnels. In Proceedings of the 2nd International Symposium on Submerged Floating Tunnels and Underwater Tunnel Structures (SUFTUS), Chongqing, China, 16–18 December 2016; pp. 180–189.
11. Bocci, E.; Graziani, A.; Canestrari, F. Mechanical 3D characterization of epoxy asphalt concrete for pavement layers of orthotropic steel decks. *Constr. Build. Mater.* **2015**, *79*, 145–152. [CrossRef]
12. Budzinski, B.; Mieczkowski, P.; Slowik, M.; Mielczarek, M.; Bilski, M.; Fornalczyk, S. Assessment of the low-temperature performance of asphalt mixtures for bridge pavement. *Road Mater. Pavement Des.* **2023**, *24*, 409–423. [CrossRef]
13. Graczyk, M.; Zbiciak, A.; Michalczyk, R.; Kowalewski, L. Numerical modelling of bubbles formation in the bridge asphalt pavement under gas pressure impact. *Transp. Res. Proc.* **2016**, *14*, 3925–3934. [CrossRef]
14. Zou, G.L.; Xu, X.Y.; Li, J.X.; Yu, H.Y.; Wang, C.J.; Sun, J. The Effects of Bituminous Binder on the Performance of Gussasphalt Concrete for Bridge Deck Pavement. *Materials* **2020**, *13*, 364. [CrossRef]
15. Shi, C. Research on Causes and Maintenance Measures of High Speed Bridge Damage in Liaoning Province. Master's Thesis, Chang'an University, Xi'an, China, 2017.
16. Tianyu, C. Analysis of deck pavement disease of hollow slab Bridge in Alpine region. *Smart Cities* **2021**, *7*, 69–70. [CrossRef]
17. Guanhua, H.; Liting, Z.; Yapeng, Y.; Mengrou, Y. Asphaltic Concrete bridge Deck paving mechanism and prevention measures. *Highway* **2019**, *64*, 21–25.
18. Fuxing, R. Causation analysis of asphalt concrete bridge deck whitening disease. *Commun. World* **2018**, *8*, 103–104. [CrossRef]
19. Chao, H. A brief discussion on the whitening pulp disease of asphalt concrete bridge deck pavement. *Heilongjiang Sci. Technol. Inf.* **2013**, *25*, 230.
20. Renjie, Q.; Lin, Z.; Cao, S.; Bin, L.; Ming, S. Causes and solutions of AC-20 whitening in the middle surface layer of Guilai Ex-pressway. *Highw. Automob. Transp.* **2015**, *5*, 119–121.
21. Yang, Y.M.; Qian, Z.D.; Song, X. A pothole patching material for epoxy asphalt pavement on steel bridges: Fatigue test and numerical analysis. *Constr. Build. Mater.* **2015**, *94*, 299–305. [CrossRef]
22. Aiguo, L.; Yang, L.; Xicai, M. Analysis of seepage causes and control technology of asphalt pavement layer of cement concrete bridge deck. *Highw. Transp. Sci. Technol. (Appl. Technol. Ed.)* **2012**, *8*, 59–61.
23. Hao, P.W.; Zhang, M.Y.; Zhang, Q.; Xu, J.Z.; Dong, S. Study on evaluation method of mud-pumping of cement concrete bridge deck pavement. *Constr. Build. Mater.* **2018**, *167*, 106–114. [CrossRef]
24. Tarefder, R.A.; Ahmad, M. Evaluation of pore structure and its influence on permeability and moisture damage in asphalt concrete. *Int. J. Pavement Eng.* **2017**, *18*, 274–283. [CrossRef]
25. Fu, J.C.; Shen, A.Q.; Zhang, H. Study on the Influence and Law of Waterproof System Design Factors on the Typical Stress of Bridge Deck Pavement. *Coatings* **2021**, *11*, 1540. [CrossRef]
26. Haynes, M.A.; Coleri, E.; Obaid, I. Performance of Waterproofing Membranes to Protect Concrete Bridge Decks. *Transp. Res. Rec.* **2021**, *2675*, 1693–1706. [CrossRef]
27. Wang, J.W.; Ji, B.F.; Chen, B.; Chen, S.Q. Application of High-Viscosity Modified Asphalt Mixture in Curved Bridge Pavement. *Sustainability* **2023**, *15*, 3411. [CrossRef]
28. Gao, Y. Causation analysis and treatment suggestion of asphalt surface of a highway bridge in Gansu Province. *Gansu Sci. Technol.* **2022**, *38*, 19–23.
29. Haimin, S. Analysis of the causes of asphalt pavement whitening based on surface energy. *Hei-Longjiang Transp. Sci. Technol.* **2019**, *42*, 91–93. [CrossRef]

30. Chao, Z. Key points and Technical Analysis of Fujian high-speed Asphalt Pavement Maintenance Engineering Design. *Fujian Transp. Sci. Technol.* **2021**, *1*, 6–8.
31. Xiong, Z.; Ningbo, L.; Peiwen, H.; Yujing, W.; Shaohui, L. Evaluation method and influencing factors of anti-whitening performance of asphalt mixture for bridge deck pavement. *Inn. Mong. Highw. Transp.* **2021**, *6*, 9–16. [CrossRef]
32. Zhiyong, H.; Chunlong, X.; Weixiong, L.; Wen, N.; Jiangmiao, Y. Analysis and control of caustic flooding mechanism of newly built asphalt pavement. *Highway* **2019**, *64*, 40–47.
33. Hu, J.; Qian, Z.D.; Liu, P.F.; Wang, D.W.; Oeser, M. Investigation on the permeability of porous asphalt concrete based on microstructure analysis. *Int. J. Pavement Eng.* **2020**, *21*, 1683–1693. [CrossRef]
34. Li, W.X.; Wang, D.Y.; Xiong, C.L.; Yu, J.M.; Chen, B.; Yu, X.S. Mechanism, prevention and remedy of alkali-pumping in new constructed asphalt pavement. *Int. J. Pavement Eng.* **2022**, *23*, 2689–2702. [CrossRef]
35. Sasaki, I.; Moriyoshi, A.; Tsunekawa, M. Water accumulation and behavior of surfactant associated with moisture permeation in bituminous pavement on concrete deck bridge. *J. Jpn. Pet. Inst.* **2006**, *49*, 315–320. [CrossRef]
36. Xu, S.F.; Lu, G.Y.; Hong, B.; Jiang, X.Y.; Peng, G.; Wang, D.W.; Oeser, M. Experimental investigation on the development of pore clogging in novel porous pavement based on polyurethane. *Constr. Build. Mater.* **2020**, *258*, 12–37. [CrossRef]
37. Jahandari, S.; Tao, Z.; Saberian, M.; Shariati, M.; Li, J.; Abolhasani, M.; Kazemi, M.; Rahmani, A.; Rashidi, M. Geotechnical properties of lime-geogrid improved clayey subgrade under various moisture conditions. *Road. Mater. Pavement* **2022**, *23*, 2057–2075. [CrossRef]
38. Toghroli, A.; Shariati, M.; Sajedi, F.; Ibrahim, Z.; Koting, S.; Mohamad, E.T.; Khorami, M. A review on pavement porous concrete using recycled waste materials. *Smart Struct. Syst.* **2018**, *22*, 433–440. [CrossRef]
39. Larsen, T.; Randhol, P.; Lioliou, M.; Josang, L.O.; Ostvold, T. Kinetics of $CaCO_3$ scale formation during core flooding. In Proceedings of the 9th International Conference on Oilfield Scale 2008—"Managing Scale Through the Field Lifetime", Aberdeen, UK, 28–29 May 2008; pp. 162–173.
40. Charpentier, T.V.J.; Neville, A.; Baraka-Lokmane, S.; Hurtevent, C.; Ordonez-Varela, J.R.; Nielsen, F.M.; Eroini, V.; Olsen, J.H.; Ellingsen, J.A.; Bache, O. Evaluation of anti-fouling surfaces for prevention of mineral scaling in sub-surface safety valves. In Proceedings of the SPE International Conference and Exhibition on Oilfield Scale 2014, Aberdeen, UK, 14–15 May 2014; pp. 31–45.
41. Foroutan, S.; Moghadasi, J. A neural network approach to predict formation damage due to calcium sulphate precipitation. In Proceedings of the SPE European Formation Damage Conference and Exhibition 2013: Unconventional and Conventional Solutions to Challenging Reservoirs, Noordwijk, The Netherlands, 5–7 June 2013; pp. 714–725.
42. Gao, C.Q. Study on the Regularity of Groundwater Crystallization Clogging Drainage Pipe and Its Influence on the Stability of High Slope. Ph.D. Thesis, Chongqing Jiaotong University, Chongqing, China, 2020.
43. Liu, Y.Y.; Lai, H.P.; Zhao, Y.B.; Sun, W.X. Spatio-Temporal Variation of Crystallites and Water Environment and Crystallization Path Analysis in Tunnel Drainage System of Calcium-Rich Surrounding Rock. *Mod. Tunn. Technol.* **2023**, 1–10. Available online: http://kns.cnki.net/kcms/detail/51.1600.U.20230331.1343.006.html (accessed on 14 May 2023).
44. Wu, Y.Z.; Li, G.P.; Jia, Q.Q.; Qi, H.Y.; Li, D.W. Study on the component characteristics and sources of porous crystallites in loess tunnel. *Mod. Tunn. Technol.* **2020**, *57*, 154–159. [CrossRef]
45. Jiang, X.; Mu, S.; Liu, J.P. Influence of chlorides and salt concentration on salt crystallization damage of cement-based materials. *J. Build. Eng.* **2022**, *61*, 105260. [CrossRef]
46. Yang, S.Y.; Han, M.; Chen, X.L.; Song, J.J.; Yang, J.S. Influence of sulfate crystallization on bond-slip behavior between deformed rebar and concrete subjected to combined actions of dry-wet cycle and freeze-thaw cycle. *Constr. Build. Mater.* **2022**, *345*, 128368. [CrossRef]

Disclaimer/Publisher's Note: The statements, opinions and data contained in all publications are solely those of the individual author(s) and contributor(s) and not of MDPI and/or the editor(s). MDPI and/or the editor(s) disclaim responsibility for any injury to people or property resulting from any ideas, methods, instructions or products referred to in the content.